

## TRANSMISSION UPPER BOUND OF PLANAR SINGLE-LAYER FREQUENCY SELECTIVE SURFACE

M.-J. Huang <sup>†</sup>

Beijing Aeronautical Technology Research Center  
Beijing 100076, China

M.-Y. Lv and Z. Wu

School of Aeronautic Science and Engineering  
Beijing University of Aeronautics and Astronautics  
Beijing 100191, China

**Abstract**—In this study, the transmission of planar single-layer frequency selective surface (FSS) has been studied using modal analysis method, and the maximum transmission that a planar single-layer FSS structure with an infinitely thin array can reach is presented. The results show that this transmission upper limit is independent of the array and the element, which indicates that it is impossible to achieve a transmission higher than this upper limit under a given incident and dielectric-supporting condition by the design of the periodic array. As the modal analysis method is an accurate method to solve the scattering problem of planar FSS with an infinitely thin array, this upper limit is also independent of the solution method. Results of both numerical simulations and experiments show that the upper limit presented in this paper is strict, but may be hard to attain when FSS is supported by lossy dielectric mediums.

### 1. INTRODUCTION

Frequency selective surfaces (FSSs) are widely used as filters from microwave band to infrared band [1–6]. Inband transmission is one of the most important design indices of those filters, such as FSS

---

*Received 27 April 2010, Accepted 25 June 2010, Scheduled 9 July 2010*

Corresponding author: M.-J. Huang (huangminjiebuaa@163.com).

<sup>†</sup> Also with School of Aeronautic Science and Engineering, Beijing University of Aeronautics and Astronautics, Beijing 100191, China.

radomes [5, 6]. Generally, a higher inband transmission is better for a band-pass FSS. It is well known that the transmission strictly equals 1 when a free-standing metal screen, perforated periodically with apertures, resonates without grating-lobe propagating. However, those free-standing FSSs have limited application for their bad mechanical properties. Nevertheless, a dielectric substrate is usually necessary for a practical FSS structure [1, 2, 7]. Furthermore, the requirements of bandwidth, angle stability, dual-polarized characteristic, as well as environmental and mechanical performance need FSSs of some functional medium coatings. The electromagnetic behaviors of FSS will be seriously influenced by these medium coatings [1, 2, 7]. In this paper, a short review of the research on the effect of the dielectric mediums on the electromagnetic behaviors is presented, along with the focus on the transmission performance of single-layer FSS.

Dielectric layers are viewed as one of the most important factors of the electromagnetic performance of FSSs besides the shape of the array, and have been investigated for several decades [7–21]. Luebbers and Munk investigated the effect of a covering layer on the resonance frequency, bandwidth, and their angle stability of an array of narrow rectangular slots. They noted that with proper design, the angle stability of the resonance frequency and bandwidth could be improved by the dielectric layers; however, some other effects might be encountered, such as a reduction in the frequency of resonance and Wood's anomaly (surface wave) null [8]. In an earlier study [9], Munk and Fulton demonstrated a double-layer FSS design that had an almost perfect frequency response achieved by appropriately arranging the dielectric layers. Callaghan, Parker, and Langley investigated the change in the resonance frequency, bandwidth, and the shape of transmission/reflection curves with the increase in the dielectric thickness. Both the cases of arrays bonded on one side and embedded centrally in the dielectrics were considered, and some important conclusions were presented [10]. Munk and Wu summarized the effects of the dielectrics on the electromagnetic performance of single-layer and multilayer FSSs, based on previous works [2, 11]. Nowadays, the design work of FSS has become increasingly complicated and novel FSS structures are being continuously developed. However, dielectrics are still playing important roles in those novel FSS structures, such as active FSSs, tunable FSSs, dielectric periodic structures, and so on [12–18]. Many researchers are still devoted to improve the electromagnetic characteristic of FSSs using dielectrics for their irreplaceable ability [19–21].

Although there is an overall understanding about the effects of dielectrics on FSSs, we still need to find out solutions to some problems.

Compared with resonance frequency, bandwidth, and the shape of the transmission/reflection curves, the effects on the transmission and reflection performance have attracted little attention. Barlevy and Rahmat-Samii investigated the reflection analytic constraints of a dielectric substrate-supported aperture array. They noted that there was a theoretical limit on the amount of energy that can be lost and this theoretical limit can be predicted by an approach presented in an earlier study [22]. They also pointed out that their analysis could be extended to any number of substrates and superstrates, but cannot be extended to multiple periodic surfaces. Generally, there are too few progresses in the effect of dielectrics on the transmission to satisfy the requirements of FSSs design. Considering these, this paper focuses on the effects of dielectrics on single-layer FSSs and attempts to provide an analytic constraint for the effects.

It can be easily observed that the transmission upper limit determined by the law of energy conservation equals 1 for a periodic array without any dielectrics, irrespective of the design of the array and element. Therefore, we presumed that dielectric-loaded FSSs may also have a similar transmission upper limit, which is independent of the shape of the array and element, and carried out our study based on this presumption. Modal analysis method (MAM), which can also be called as the mode-matching method, was employed to solve the FSS problem.

In this paper, a derivation of the transmission upper limit of the single-layer FSS with an infinitely thin array is presented in Section 2, based on the analysis of energy conservation, and testing the reliability and practicability of this upper limit, presented in Section 3. In Section 4, the applicable condition is discussed. Lastly, in Section 5, some possible applications of the transmission upper limit are given.

## 2. DERIVATION OF THE TRANSMISSION UPPER LIMIT

### 2.1. Modal Analysis Method [1, 23, 24]

Figure 1(a) shows an FSS structure comprising of  $M$  dielectric superstrates and  $N$  substrates. The array at  $z = z_M$  is assumed to be infinitely thin and perfect conductive. The FSS is of infinite extent in both  $x$ - and  $y$ -directions but has a thickness in  $z$ -direction. The shape of the array is shown in Fig. 1(b). Modal analysis method gives the tangential fields in the dielectric mediums as series of Floquet modes,

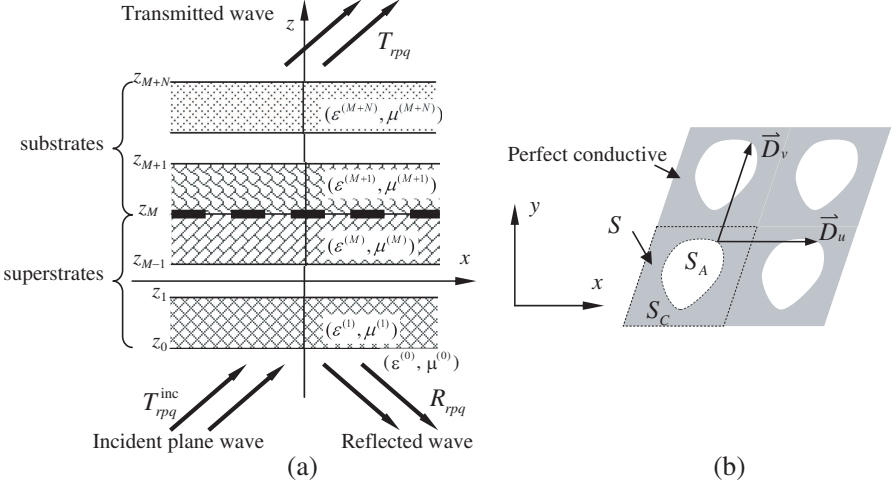


**Figure 1.** Description of a single-layer FSS. (a)  $z$ - $x$  cross section of a single-layer FSS with  $M$  dielectric superstrates and  $N$  substrates. (b)  $x$ - $y$  view of an arbitrary aperture array.

as  $z_{n-1} \leq z \leq z_n$ :

$$\begin{cases} \vec{E}_t^{(n)} = \sum_{r=0}^1 \sum_{p,q=-\infty}^{+\infty} \left( T_{rpq}^{(n)} e^{-i\gamma_{pq}^{(n)} z} + R_{rpq}^{(n)} e^{i\gamma_{pq}^{(n)} z} \right) \vec{A}_{rpq}(\vec{r}_t) \\ \vec{H}_t^{(n)} = \sum_{r=0}^1 \sum_{p,q=-\infty}^{+\infty} \xi_{rpq}^{(n)} \left( T_{rpq}^{(n)} e^{-i\gamma_{pq}^{(n)} z} - R_{rpq}^{(n)} e^{i\gamma_{pq}^{(n)} z} \right) \hat{z} \times \vec{A}_{rpq}(\vec{r}_t) \end{cases} \quad (1)$$

where  $\vec{A}_{rpq}(\vec{r}_t)$  is the vector Floquet mode,  $\gamma_{pq}^{(n)}$  is the normal component of the wave vector, while  $T_{rpq}^{(n)}$  and  $R_{rpq}^{(n)}$  are the transmission and reflection coefficients of the  $rpq$ th order field, respectively. The superscript “ $(n)$ ” indicates the  $n$ th layer. The subscript “ $r$ ” is the polarization, while “ $p$ ” and “ $q$ ” are the two coefficients of the Floquet mode. Considering the continuity of the tangential field on the interface between two dielectric media, we can obtain:

$$\begin{bmatrix} T_{rpq}^{(M)} \\ R_{rpq}^{(M)} \end{bmatrix} = \mathbf{\Gamma}_{rpq}^{(M,0)} \begin{bmatrix} T_{rpq}^{(0)} \\ R_{rpq}^{(0)} \end{bmatrix} = \mathbf{\Gamma}_{rpq}^{(M,0)} \begin{bmatrix} T_{rpq}^{\text{inc}} \\ R_{rpq} \end{bmatrix} \quad (2a)$$

$$\begin{bmatrix} T_{rpq}^{(M+1)} \\ R_{rpq}^{(M+1)} \end{bmatrix} = \mathbf{\Gamma}_{rpq}^{(M+1,M+N+1)} \begin{bmatrix} T_{rpq}^{(M+N+1)} \\ R_{rpq}^{(M+N+1)} \end{bmatrix} = \mathbf{\Gamma}_{rpq}^{(M+1,M+N+1)} \begin{bmatrix} T_{rpq} \\ 0 \end{bmatrix} \quad (2b)$$

where

$$\Gamma_{rpq}^{(m,n)} = \begin{cases} \prod_{i=1}^{n-m} \left( \mathbf{M}_{0rpq}^{(m-1+i)} \right)^{-1} \mathbf{M}_{1rpq}^{(m-1+i)} & n > m \\ \prod_{i=1}^{m-n} \left( \mathbf{M}_{1rpq}^{(m-i)} \right)^{-1} \mathbf{M}_{0rpq}^{(m-i)} & n < m \\ \mathbf{I} & m = n \end{cases}$$

$$\mathbf{M}_{0rpq}^{(n)} = \begin{bmatrix} e^{-i\gamma_{pq}^{(n)} z_n} & e^{i\gamma_{pq}^{(n)} z_n} \\ \xi_{rpq}^{(n)} e^{-i\gamma_{pq}^{(n)} z_n} & -\xi_{rpq}^{(n)} e^{i\gamma_{pq}^{(n)} z_n} \end{bmatrix}$$

$$\mathbf{M}_{1rpq}^{(n)} = \begin{bmatrix} e^{-i\gamma_{pq}^{(n+1)} z_n} & e^{i\gamma_{pq}^{(n+1)} z_n} \\ \xi_{rpq}^{(n+1)} e^{-i\gamma_{pq}^{(n+1)} z_n} & -\xi_{rpq}^{(n+1)} e^{i\gamma_{pq}^{(n+1)} z_n} \end{bmatrix}$$

We can define the inner product on the array's unit cell as:

$$\langle \vec{F}(\vec{r}_t), \vec{G}(\vec{r}_t) \rangle = \iint_S \vec{F}(\vec{r}_t) \cdot \vec{G}^*(\vec{r}_t) ds \quad (3)$$

By expanding the unknown aperture electric field  $\vec{E}_A(\vec{r}_t)$  in terms of Floquet modes, and matching both the electric- and magnetic field boundary condition at  $z = z_M$ :

$$\vec{E}_t^{(M)} = \vec{E}_t^{(M+1)} = \vec{E}_A = \begin{cases} \vec{E}_A & \vec{r}_t \in S_A \\ 0 & \vec{r}_t \in S_C \end{cases} \quad (4a)$$

$$\vec{H}_t^{(M)} = \vec{H}_t^{(M+1)} \quad \vec{r}_t \in S_A \quad (4b)$$

we obtain:

$$\sum_{r=0}^1 \sum_{p,q=-\infty}^{+\infty} \left( \frac{\Omega_{rpq,21}^+}{\Omega_{rpq,11}^+} - \frac{\Omega_{rpq,22}^-}{\Omega_{rpq,12}^-} \right) E_{rpq} \vec{A}_{rpq}(\vec{r}_t)$$

$$= \sum_{r=0}^1 \sum_{p,q=-\infty}^{+\infty} \left( \Omega_{rpq,21}^- - \Omega_{rpq,22}^- \frac{\Omega_{rpq,11}^-}{\Omega_{rpq,12}^-} \right) T_{rpq}^{\text{inc}} \vec{A}_{rpq}(\vec{r}_t) \quad \vec{r}_t \in S_A \quad (5)$$

where

$$E_{rpq} = \langle \vec{E}_A(\vec{r}_t), \vec{A}_{rpq}(\vec{r}_t) \rangle / S = \frac{1}{S} \iint_S \vec{E}_A(\vec{r}_t) \cdot \vec{A}_{rpq}^*(\vec{r}_t) ds \quad (6)$$

$$\Omega_{rpq}^- = \mathbf{M}_{0rpq}^{(M)} \Gamma_{rpq}^{(M,0)}, \quad \Omega_{rpq}^+ = \mathbf{M}_{1rpq}^{(M)} \Gamma_{rpq}^{(M+1,M+N+1)}$$

The subscript “ $ij$ ” of  $\Omega_{rpq,ij}^+$  and  $\Omega_{rpq,ij}^-$  indicates the element of the  $i$ th row and  $j$ th column of a matrix, respectively.

Equation (5) is known as the magnetic field integral equation (MFIE) of an aperture array, and can be solved with method of moments (MoMs). The method of moments begins by expressing  $\vec{E}_A(\vec{r}_t)$  in terms of a set of known basis functions  $\{\vec{F}_n(\vec{r}_t)\}$ :

$$\vec{E}_A(\vec{r}_t) = \sum_{n=1}^{C_m} x_n \vec{F}_n(\vec{r}_t)$$

$$E_{rpq} = \langle \vec{E}_A, \vec{A}_{rpq} \rangle / S = \sum_{n=1}^{C_m} x_n \langle \vec{F}_n(\vec{r}_t), \vec{A}_{rpq} \rangle / S = \sum_{n=1}^{C_m} x_n F_{n,rpq} \quad (7)$$

where  $\{x_n\}$  are the unknown coefficients to be determined. Substituting it into (5) and taking the inner product with every basis function, MFIE given in (5) is thus converted to a matrix equation:

$$\mathbf{Y}\mathbf{x} = \mathbf{b} \quad (8)$$

where

$$\mathbf{Y} = [Y_{mn}]_{m,n}, \quad \mathbf{b} = [b_m]_m, \quad \mathbf{x} = [x_n]_n$$

$$Y_{mn} = \sum_{r=0}^1 \sum_{p,q=-\infty}^{+\infty} (C_{rpq} F_{n,rpq} F_{m,rpq}^*),$$

$$b_m = \sum_{r=0}^1 \sum_{p,q=-\infty}^{+\infty} (D_{rpq} T_{rpq}^{inc} F_{m,rpq}^*)$$

$$C_{rpq} = \frac{\Omega_{rpq,21}^+}{\Omega_{rpq,11}^+} - \frac{\Omega_{rpq,22}^-}{\Omega_{rpq,12}^-}, \quad D_{rpq} = \Omega_{rpq,21}^- - \Omega_{rpq,22}^- \frac{\Omega_{rpq,11}^-}{\Omega_{rpq,12}^-}$$

Correspondingly, the transmission and reflection coefficients are given by:

$$\begin{bmatrix} T_{rpq} \\ R_{rpq} \end{bmatrix} = \begin{bmatrix} 1/\Omega_{rpq,11}^+ \\ 1/\Omega_{rpq,12}^- \end{bmatrix} \sum_{m=1}^{C_m} x_m F_{m,rpq} - \begin{bmatrix} 0 \\ \Omega_{rpq,11}^-/\Omega_{rpq,12}^- \end{bmatrix} T_{rpq}^{inc} \quad (9)$$

## 2.2. Energy Conservation and Resonance in Modal Analysis Method

According to the definition of inner product described in (3), both  $\vec{F}(\vec{r}_t)$  and  $\vec{G}(\vec{r}_t)$  are vectors defined on the unit cell. Thus, (3) can be rewritten as:

$$\langle \vec{F}(\vec{r}_t), \vec{G}(\vec{r}_t) \rangle = \hat{z} \cdot \iint_S [\vec{F}(\vec{r}_t) \times \hat{z}] \times \vec{G}^*(\vec{r}_t) ds$$

The MFIE given in (5) describes the continuity of the aperture magnetic, which is equal to

$$\vec{H}_t^{(M)} \times \hat{z} = \vec{H}_t^{(M+1)} \times \hat{z} \quad \vec{r}_t \in S_A \quad (10)$$

In the process of converting (10) into matrix equation, the left-hand side of the equation signifies

$$\left\langle \vec{H}_t^{(M)} \times \hat{z}, \vec{F}_n \right\rangle = \hat{z} \cdot \iint_S \vec{F}_n^* \times \vec{H}_t^{(M)} ds = 2S_z^* \left( \vec{F}_n, \vec{H}_t^{(M)} \right) \quad (11)$$

It can be regarded as the average power produced by the aperture magnetic field ( $\vec{H}_t^{(M)}$ ) on the  $-z$  side of the array, and taken by the  $n$ th basis electric field ( $\vec{F}_n$ ) on a unit cell. The physical meaning of the right-hand side of (10) is similar, and thus, the matrix Equation (8) gives a component form of the energy conservation on a unit cell.

If the incident polarization state is represented by “ $R$ ”, then  $T_{rpq}^{\text{inc}} = \delta_{0p}\delta_{0q}\delta_{Rr}$ . By left multiplying both the sides of (8) by the unknown vector  $\mathbf{x}^H$ , we obtain:

$$\sum_{r=0}^1 \sum_{p,q=-\infty}^{+\infty} C_{rpq} (\mathbf{F}_{rpq}^T \mathbf{x})^H (\mathbf{F}_{rpq}^T \mathbf{x}) = D_{R00} (\mathbf{F}_{R00}^T \mathbf{x})^H \quad (12)$$

where

$$\mathbf{F}_{rpq} = [ F_{1,rpq} \quad F_{2,rpq} \quad \dots \quad F_{C_m,rpq} ]^T$$

As  $E_{rpq} = \mathbf{F}_{rpq}^T \mathbf{x}$ , (12) can be simplified to

$$\sum_{r=0}^1 \sum_{p,q=-\infty}^{+\infty} C_{rpq} |E_{rpq}|^2 = D_{R00} E_{000}^* \quad (13)$$

Equation (13) is the full form of the energy conservation, which signifies the average scattered power of the aperture field is equal to the average incident power taken by the aperture electric field on a unit cell.

With respect to the no dielectric case, we know that

$$\Omega_{rpq}^- = \Omega_{rpq}^+ = \begin{bmatrix} 1 & 1 \\ \xi_{rpq} & -\xi_{rpq} \end{bmatrix}, \quad C_{rpq} = D_{rpq} = 2\xi_{rpq}$$

By substituting them and (9) into (13), we obtain

$$\sum_{r=0}^1 \sum_{p,q=-\infty}^{+\infty} \xi_{rpq} |T_{rpq}|^2 = \xi_{R00} T_{R00}^* \quad (14)$$

As cross-polarization fundamental mode of the scattered field should be 0, the basis functions and the aperture electric field must satisfy the following equation:

$$T_{!R00} = E_{!R00} = \mathbf{x}^T \mathbf{F}_{!R00} = \mathbf{F}_{!R00}^T \mathbf{x} = 0 \quad (15)$$

where the subscript “!R00” indicates the cross-polarization mode of R00.

With regard to the definition of the modal admittance, we know that every  $\xi_{rpq}$  corresponds to an energy mode. The mode is a pure propagation mode when  $\xi_{rpq}$  is real, and it is a pure evanescent mode when  $\xi_{rpq}$  is imaginary. If  $\xi_{rpq}$  is a complex number, it corresponds to a propagation mode, which has some dissipation. There are only two kinds of modes in the free space: pure propagation modes and pure evanescent modes. The  $\xi_{r00}$  corresponds to the fundamental mode (main lobe), and  $\xi_{rpq}(pq \neq 00)$  corresponds to the upper mode. If  $\xi_{rpq}(pq \neq 00) \in \mathbb{R}$ , then the upper mode will take a part of energy, and is known as the grating lobe. If no grating lobe appears, then  $\xi_{rpq}(pq \neq 00) \in \mathbb{I}$ , and (14) can be written as a summation of propagation modes and evanescent modes, as

$$\xi_{R00} |T_{R00}|^2 + \sum_{rpq \neq r00} \xi_{rpq} |T_{rpq}|^2 = \xi_{R00} T_{R00}^* \quad (16)$$

The first part of the left-hand side of (16) is the traveling wave component of the average power density of the transmitted field on a unit cell, and the second part is the average power density in the form of standing waves. The right-hand side of (16) is the incident power density taken by the aperture field. As the second part of the left-hand side of (16) is pure imaginary and  $\xi_{r00}$  is real, the solution of (16) must have the form of

$$T_{R00} = (1 + \alpha)/2 \quad (17)$$

and

$$\sum_{rpq \neq r00} \xi_{rpq} |T_{rpq}|^2 = 0 \Leftrightarrow T_{R00} = 1 \quad (18a)$$

$$T_{R00} = 0 \Rightarrow \left\| \sum_{rpq \neq r00} \xi_{rpq} \mathbf{F}_{rpq}^* \mathbf{F}_{rpq}^T \right\| \rightarrow +\infty \quad (18b)$$

where  $\alpha$  is the unit complex.

Equation (17) shows the track of the fundamental mode transmission coefficient  $T_{R00}$  to the frequency (Fig. 2). This result can also be obtained by other analyzing method, such as

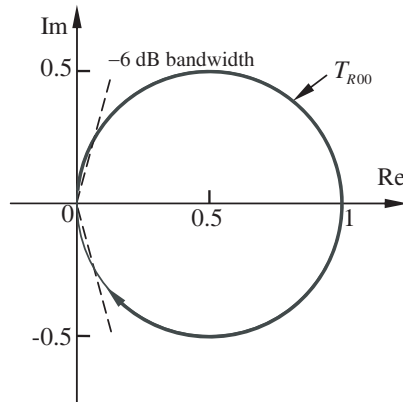


**Figure 2.** Track of  $T_{R00}$  of a free-standing single-layer FSS.

equivalent transmission line theory, equivalent circuit theory and mutual impedance approach by Munk [2].

As the real part of the complex Poynting vector indicates the traveling wave component of the energy flux density, and the imaginary part indicates the standing wave component, Equation (18a) shows the energy performance of resonance — the standing component of the power scattered by the aperture field equal to 0 at resonance. The transmission null given by (18b) is known as “Wood’s anomaly,” which indicates the mode change of the aperture-field distribution [2, 8, 24–26].

For our convenience, we define the resonance of dielectric-loaded single-layer FSS with reference to the free-standing case, such that both sides of (13) are real numbers or the standing wave component of the power scattered by the aperture field equals 0.

### 2.3. Transmission Upper Limit of Dielectric-loaded FSS

According to the energy definition of resonance, the standing wave component of the power scattered by the aperture field equals 0 for a dielectric-loaded FSS. Hence:

$$C_{R00,Im} |E_{R00}|^2 + \sum_{rpq \neq 0pq} C_{rpq,Im} |E_{rpq}|^2 = 0 \quad (19a)$$

$$C_{R00,Re} |E_{R00}|^2 + \sum_{rpq \neq 0pq} C_{rpq,Re} |E_{rpq}|^2 = D_{R00} E_{R00}^* \quad (19b)$$

Expressions (19a) and (19b) describe the energy conservation of FSS in the standing and traveling component form separately.

It is easy to prove by mathematical induction that all signs of  $C_{rpq,\text{Re}}$  are the same. Hence, (19b) implicates:

$$\begin{aligned} |C_{R00,\text{Re}}| |E_{R00}|^2 &\leq |C_{R00,\text{Re}}| |E_{R00}|^2 + \sum_{rpq \neq r00} C_{rpq,\text{Re}} |E_{rpq}|^2 \\ &= |D_{R00} E_{R00}^*| \Rightarrow |E_{R00}| \leq |D_{R00}| / |C_{R00,\text{Re}}| \end{aligned} \quad (20)$$

According to (9),  $\Omega_{rpq,11}^+$  is only related to the dielectrics and the incident condition. Therefore, by combining (9) with (20), we can obtain

$$|T_{R00}| = \left| E_{R00} / \Omega_{R00,11}^+ \right| \leq |D_{R00}| / \left| \Omega_{R00,11}^+ C_{R00,\text{Re}} \right|$$

and define

$$T_{R,\text{top}} = |D_{R00}| / \left| \Omega_{R00,11}^+ C_{R00,\text{Re}} \right| \quad (21)$$

where  $T_{R,\text{top}}$  is the transmission upper limit of single-layer FSS.

As this derivation is not relevant to the incidence condition, dielectrics, the shape of array, and aperture-field basis functions, the transmission upper limit given by (21) is suitable for any planar single-layer FSS of infinite extent. The expression shows that  $T_{R,\text{top}}$  depends on the dielectrics and the incident condition, indicating that the calculated transmission coefficient of a given FSS structure excited by certain plane wave cannot exceed  $T_{R,\text{top}}$ , if analyzed by MAM. As MAM is known to be an accurate method to solve the scattering problems of the FSSs of infinite extent, the upper limit is independent of the solving technique.

### 3. VERIFICATION AND PRACTICAL EFFECTS

#### 3.1. Testing by Simulated Results

Numerical simulation was conducted to test the reliability and practicability of the transmission upper limit given by (21). Both MAM and finite elements method (FEM) are employed to ensure that the conclusions are independent of the solving technique.

Figure 3 shows a comparison between the calculated transmission response and the upper limit of a compact cross-loop aperture array supported by a lossless dielectric superstrate for both TE and TM wave incidences at the incident angle  $\theta = 60^\circ$ . The results obtained by MAM are strictly controlled by the upper limit given by (21), and the result for TM wave incidence computed by FEM slightly exceeds the limit, but shows the same trend.

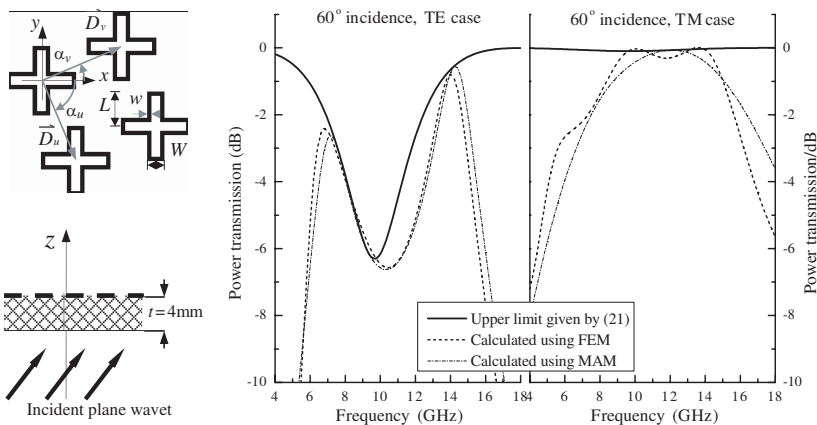


**Figure 3.** Frequency response of an FSS supported by a lossless dielectric superstrate. ( $D_u = D_v = 5$  mm,  $L = 4.5$  mm,  $w = 0.24$  mm,  $\epsilon_r = 4.5$ ).

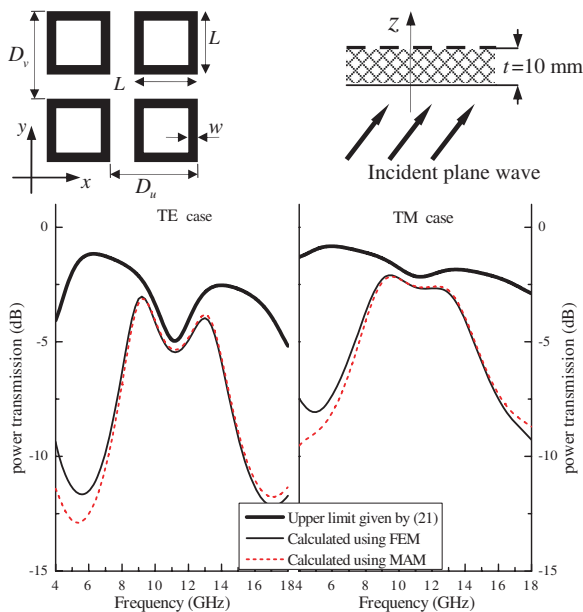


**Figure 4.** Frequency response of a rectangle-loop array supported by a lossy dielectric superstrate. ( $D_u = D_v = 5$  mm,  $L = 4.5$  mm,  $w = 0.24$  mm,  $\epsilon_r = 4.5$ ,  $\tan \delta = 0.06$ ).

As an example of the application in predicting the transmission of FSS loaded by lossy dielectric, we evaluated the frequency response of a rectangle-loop array loaded by a lossy dielectric superstrate at the incident angle  $\theta = 45^\circ$ . Both the results calculated by MAM and FEM were well constrained by (21), as shown in Fig. 4.

The dielectric symmetrically loaded FSS corresponding to Fig. 4 was also considered, and the results are presented in Fig. 5. The calculation condition and the array of Fig. 5 were the same with those given in Fig. 4. It demonstrated that the transmission upper limit of dielectric symmetrical loaded FSS is obviously higher than the dissymmetrical structure, and the transmission of the dielectric symmetrical loaded FSS calculated by MAM is still strictly lower than the upper limit.

To test the capacity of dealing with complex FSS structure, a model consisting of six lossy dielectric mediums (3 substrates and 3 superstrates) was evaluated. The parameters of those six dielectric mediums were set at random, and the incident angle was  $\theta = 30^\circ$ . Fig. 6 shows the transmission spectra of this complex FSS structure with different arrays. The results revealed that the transmission

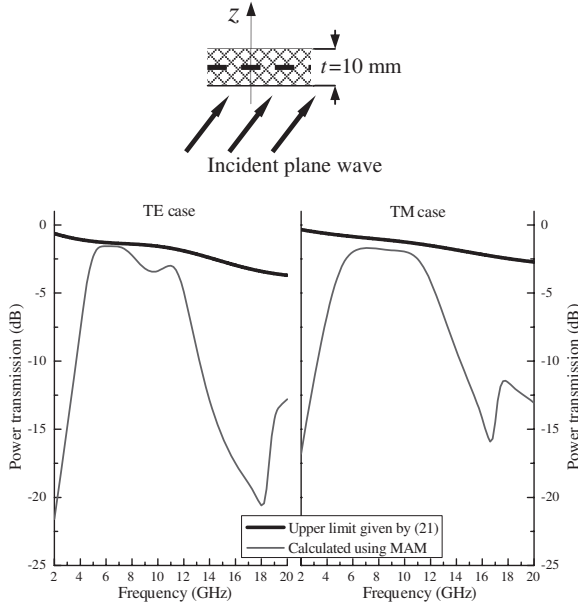


**Figure 5.** Frequency response of an FSS centrally embedded in a lossy dielectric medium. The array and dielectric are same as those given in Fig. 4.

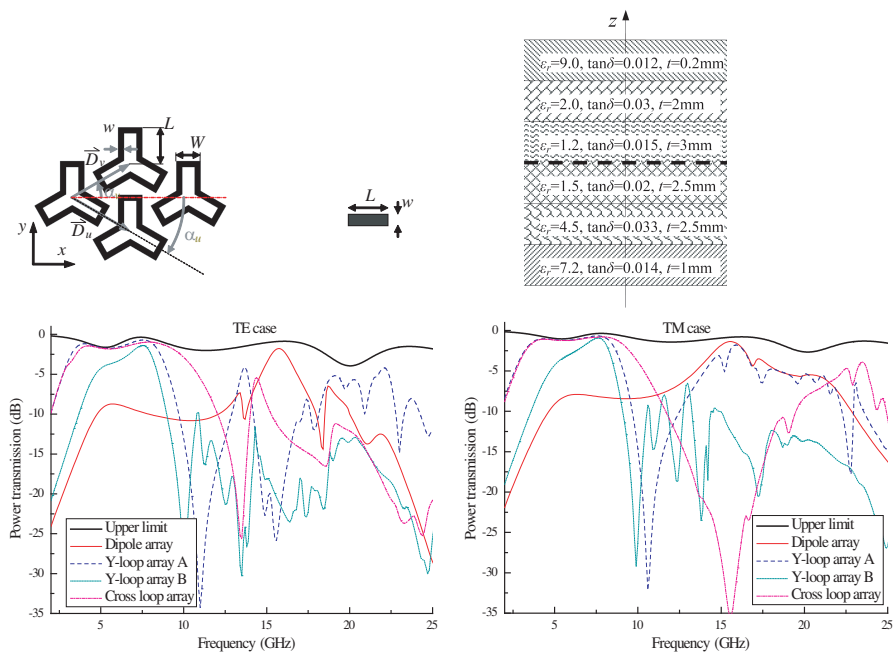


**Figure 6.** Frequency response of an FSS with six dielectric mediums. (Dipole array:  $D_u = 10$  mm,  $D_v = 5$  mm,  $\alpha_u = 0^\circ$ ,  $\alpha_v = 90^\circ$ ,  $L = 10$  mm,  $w = 0.4$  mm; Y-loop array A:  $D_u = D_v = 10$  mm,  $\alpha_u = -30^\circ$ ,  $\alpha_v = 30^\circ$ ,  $L = 7.2$  mm,  $W = 3.0$  mm,  $w = 0.5$  mm; Y-loop array B:  $D_u = D_v = 16$  mm,  $\alpha_u = -30^\circ$ ,  $\alpha_v = 30^\circ$ ,  $L = 7.2$  mm,  $W = 3.0$  mm,  $w = 0.5$  mm; Cross-loop array:  $D_u = D_v = 8$  mm,  $\alpha_u = -66.8^\circ$ ,  $\alpha_v = 23.2^\circ$ ,  $L = 5.6$  mm,  $W = 2.8$  mm,  $w = 0.5$  mm).

calculated by MAM is still constrained by the analytic constraint, though the structure is much complex. Furthermore, for an FSS consisting of lossy dielectrics, the upper limit given by (21) can be approached by adjusting the array and element, but is impossible to exceed.

### 3.2. Testing by Experimental Results

A series of experiments were conducted to give a further verification to the reliability and practicability of the transmission upper limit. The operating principle of the transmission measurement system is sketched in Fig. 7. The measured power transmission of an FSS board

is defined as:

$$T_M = \frac{S_{recv,FSS}}{S_{recv,0}} \quad (22)$$

In the above equation,  $S_{recv,FSS}$  is the received power of the receiving antenna when FSS board is laid and  $S_{recv,0}$  is the received power without FSS board.

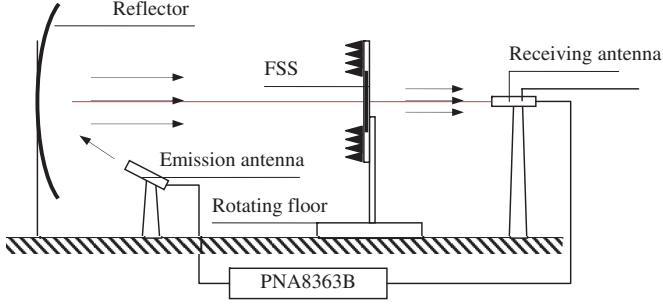


**Figure 7.** Schematic representation of the transmission measurement system.

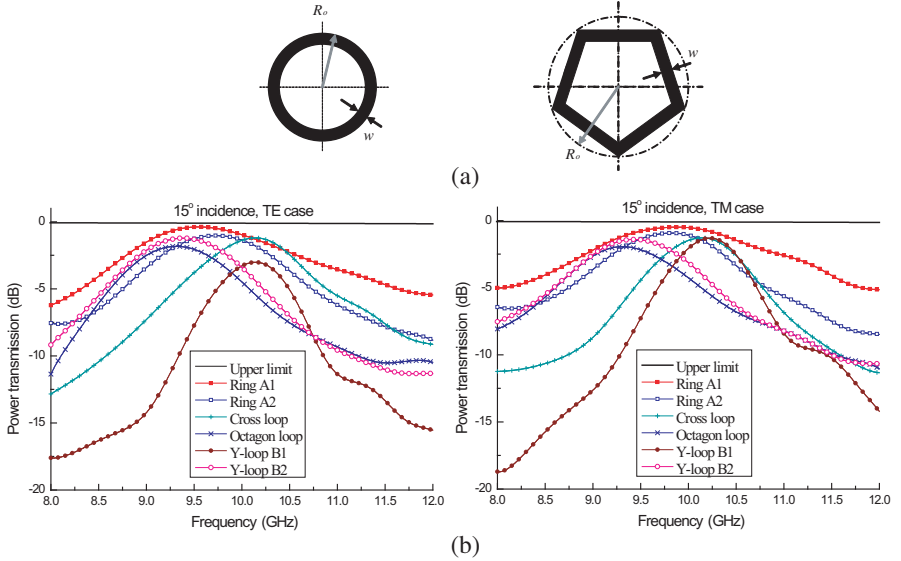


**Figure 8.** Measured frequency response of FSS samples in group A. (a) Geometries of the ring element and the regular-polygon element. (b) Comparison between the measured transmission and the transmission upper limit.

Two groups of FSS boards with different arrays printed in a dielectric substrate were fabricated. The detailed parameters of the FSS samples are listed in Table 1. Group A consists of six FSS boards which have the same dimension of 400 mm × 400 mm × 0.963 mm. The

**Table 1.** Parameters of the FSS samples.

Group	Substrate	Array	Unit Cell
A	$\epsilon_r = 4.6$ $\tan \delta = 0.02$ $t = 0.963$ mm	Ring A1	$D_u = D_v = 10.5$ mm, $\alpha = 90^\circ$ , $R_o = 3.775$ mm, $w = 0.45$ mm
		Ring A2	$D_u = D_v = 13.0$ mm, $\alpha = 90^\circ$ , $R_o = 3.775$ mm, $w = 0.45$ mm
		Cross loop	$D_u = D_v = 10.5$ mm, $\alpha = 90^\circ$ , $L = 3.275$ mm, $W = 1.85$ mm, $w = 0.35$ mm
		Octagon loop	$D_u = D_v = 13.0$ mm, $\alpha = 90^\circ$ , $R_o = 3.725$ mm, $w = 0.3$ mm
		Y-loop B1	$D_u = D_v = 12.5$ mm, $\alpha = 90^\circ$ , $L = 3.520$ mm, $W = 1.8$ mm, $w = 0.3$ mm
		Y-loop B2	$D_u = D_v = 10.5$ mm, $\alpha = 90^\circ$ , $L = 3.848$ mm, $W = 2.35$ mm, $w = 0.35$ mm
B	$\epsilon_r = 4.6$ $\tan \delta = 0.02$ $t = 1.463$ mm	Hexagon loop C1	$D_u = D_v = 15.0$ mm, $\alpha = 60^\circ$ , $R_o = 3.73$ mm, $w = 0.3$ mm
		Hexagon loop C2	$D_u = D_v = 15.0$ mm, $\alpha = 60^\circ$ , $R_o = 3.78$ mm, $w = 0.3$ mm

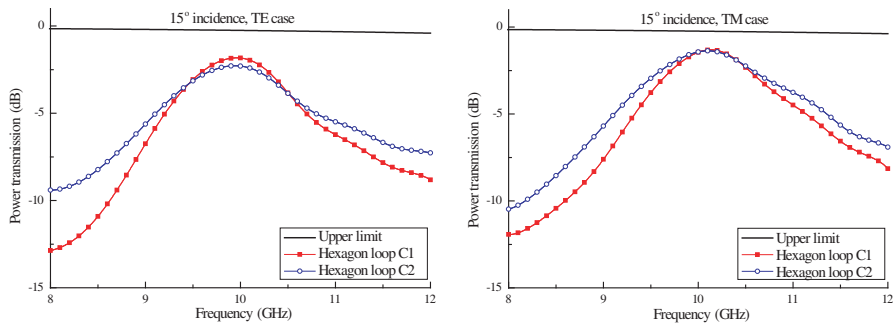


**Figure 9.** Measured frequency response of FSS samples in group B.

substrate has an approximately constant relative permittivity  $\varepsilon_r = 4.6$  and loss tangent  $\delta = 0.02$  in the frequency band 8–12 GHz. Fig. 8 shows the measured transmission response of the six FSS samples in group A illuminated by a plane wave with oblique incidence ( $\theta = 15^\circ$ ). The comparison with the transmission upper limit determined by (21) shows no exception but the theoretical upper limit is hard to attain for the arrays are not dense enough.

There are two FSS samples in group B. Both of them have the same substrate material with group A but a greater thickness  $t = 1.463$  mm. Fig. 9 shows their frequency response for both TE and TM incident waves at angle  $\theta = 15^\circ$ . The theoretical upper limit is still proved to can not be exceeded.

### 3.3. Comparison with the Performance of Corresponding Multilayer Dielectric Structure

The transmission coefficient of the multilayered dielectric structure can be easily deduced by a similar process

$$T_R = \frac{1}{\Omega_{R00,11}^+} \frac{D_{R00}}{C_{R00}} \quad (23)$$

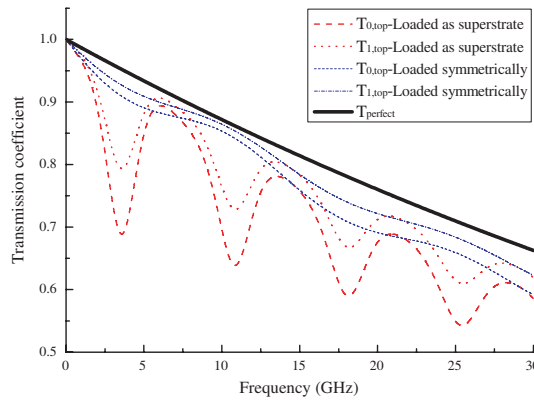
Obviously,  $|T_R| \leq |T_{R,\text{top}}|$ . This means that the transmission of FSS is still constrained by (21) even if the shape of the aperture is infinity or the aperture area ratio ( $S_{\text{aperture}}/S_{\text{unit cell}}$ ) approximates 1 (while FSS degenerates to a multilayered dielectric structure). It also shows that the presence of the conductive array significantly improves the impedance-matching performance of the dielectric structure.

Another challenge to the transmission upper limit comes from the perfect transmission of the multilayered dielectric structure. We can define the perfect transmission coefficient as the transmission coefficient in an ideal state when there is no reflection on each dielectric interface. Thus,

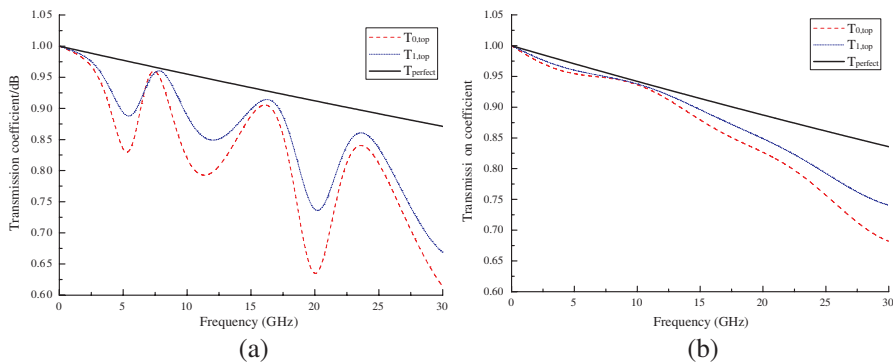
$$T_{\text{perfect}} = \left| \prod_{n=1}^{M+N} e^{-\gamma_{00}^{(n)}(z_n - z_{n-1})} \right| \quad (24)$$

Figure 10 shows a comparison between the transmission upper limit of FSSs given in Figs. 4 and 5 and the perfect transmission determined by (24). A comparison between the transmission upper limit of the FSS structure shown in Fig. 6 and the perfect transmission is present in Fig. 11(a), while the transmission of the corresponding dissymmetrical structure is compared in Fig. 11(b). Generally,

dielectric symmetrically loaded FSS has a higher transmission than the dissymmetrical one. Both Figs. 10 and 11 show that the transmission upper limit equals the perfect transmission only for a free-standing periodic surface, and that the former is lower than latter for all other cases.



**Figure 10.** Comparison between the transmission upper limit and the perfect transmission for a single-layer FSS loaded by one dielectric medium. (FSS structure with dielectric loaded as a superstrate is same as that calculated in Fig. 4, while the symmetrically loaded structure is similar to that given in Fig. 5. The incident condition is also the same as given in Fig. 6.)



**Figure 11.** Comparisons between the transmission upper limit and the perfect transmission for complex single-layer FSSs. (a) FSS structure is the same as that calculated in Fig. 6. (b) Dielectric mediums are symmetric with respect to the array, and the superstrates are same as shown in Fig. 6. Both incident conditions are also same as given in Fig. 6.

The two previously mentioned comparisons not only tested the reliability of the transmission upper limit, but also offered a general picture of the degree of interaction between the array and dielectrics.

## 4. APPLICABLE CONDITION

### 4.1. Scope of Application

Based on the derivation in Section 2, we can conclude the scope of application of the transmission upper limit given in (21) as follows:

- (1) Single-layer FSS of infinite extent.
- (2) The array is infinitely thin and perfect conductive.
- (3) A plane wave incidence.
- (4) The properties of the dielectrics do not change in the tangent direction ( $x$ - and  $y$ -directions).

Though the aperture-array assumption was made just for our convenience to match the boundary conditions for building the MFIE, because the essential of the field continuity was independent of the assumption, (21) may still be suitable for FSSs with patch array. The form of (21) signifies that if the equivalent admittances of the dielectrics ( $C_{rpq}$  and  $D_{rpq}$ ) can be obtained, then the transmission upper limit should exist. In other words, constraint (4) can be relaxed, such that the properties of the dielectrics have the same period as the array. Furthermore, if FSSs is not excited by a plane wave, then (21) can be applied by expanding the incident field in terms of plane waves.

## 5. POSSIBLE APPLICATIONS

There are many possible applications of the transmission upper limit present in this paper, such as evaluating the feasibility of a design or the reachability of a design goal, explaining some characteristics of the frequency behavior of single-layer FSS, and so on.

### 5.1. Evaluating the Feasibility of a Design or the Reachability of a Design Goal

A common misunderstanding in the design of FSS components is the design goal has been set too high to reach, or the selected form of the FSS structure is unsuitable which make it is hard to satisfy the requirements by designing the array and unit cell. The transmission upper limit present in this paper is well in solving those problems.

Figure 12 shows a possible structure form of an FSS radome. This typical form consists of an aperture array on the outer side of a medium radome and two functional coatings. A possible design state may be: coating 1 is a flashing coating of thickness  $t = 0.1$  mm, relative permittivity  $\epsilon_r = 3.0$  and loss tangent  $\tan \delta = 0.05$ , coating 2 is an anti-static coating of  $t = 0.1$  mm,  $\epsilon_r = 6.1$  and  $\tan \delta = 0.11$ , and the medium radome is made of a resin slab of  $t = 8$  mm  $\epsilon_r = 4.5$  and  $\tan \delta = 0.02$ . The design goal requires the transmission in the band of  $10 \pm 0.5$  GHz be no less than 80% at incident angle  $\theta \approx 70^\circ$ . The transmission upper limit determined by (21) has been calculated as given in Fig. 13. The results show that the transmission upper limit of the TE polarization on the required incident condition is  $\leq 78.4\%$ , which is less than the design index. This means the selected structure form of the FSS radome is infeasible which make it is impossible to satisfy the design goal by adjusting the array and element, or the

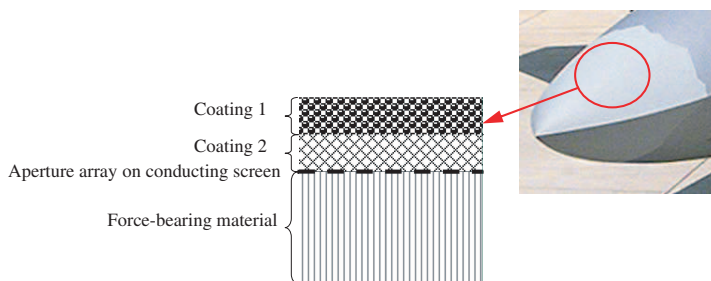


**Figure 12.** A typical structure form of the FSS radome.

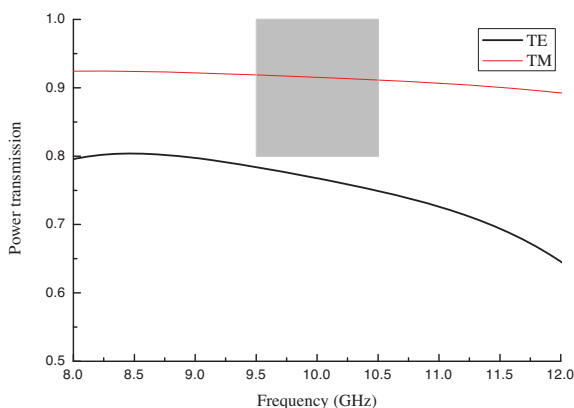


**Figure 13.** The transmission upper limit of the given structure form of the FSS radome.

design goal is too impractical to reach. Possible improvements include changing the structure form of the FSS radome, instituting the resin with some low loss and high strength materials, decreasing the design index and the combination of the above.

## 5.2. Explaining Some Characteristics of the Frequency Behavior of Single-layer FSS

Some characteristics of the frequency response of a single-layer FSS are hard to understand in other way. Fig. 14 shows the transmission-frequency curve of a single-layer FSS for normal incident. The FSS structure consists of a conducting screen perforated by a dipole array and a dielectric slab of thickness  $t = 8.6$  mm. The transmission-frequency curve shown in Fig. 14 has a “flat-top” shape and an obvious valley near the in-band center frequency, which is similar to the behaviors of a double-layer FSS. However, the mechanism of this phenomenon is much different from that of a double-layer FSS. The “flat-top” in-band characteristic is caused by the dense array of the dipole and the in-band valley is due to the mismatching of the impedance. A strong reflection is inevitable in the band of 11–15 GHz for such an FSS structure for the impedance of the dielectric slab can not match well with the wave impedance in the free space. The transmission upper limit curve in Fig. 14 shows us how badly the transmission performance influenced by the impedance mismatching. This is also the reason why authors chose the energy definition of the resonance other than the maximum transmission definition.

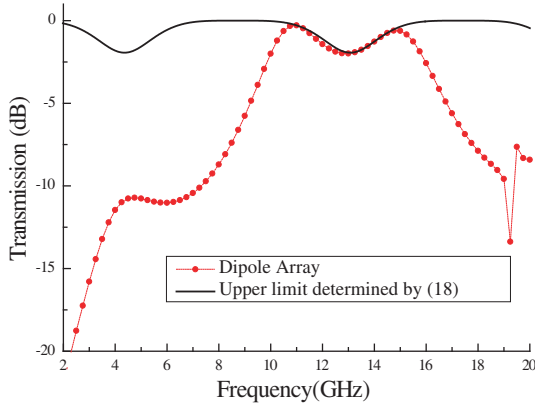


**Figure 14.** Frequency response of an infinite dipole array ( $L = 8.3$  mm,  $w = 0.3$  mm,  $D_u = 8.4$  mm,  $D_v = 3.0$  mm).

Similarly, some frequency behaviors of single-layer FSSs which have more complex structures also can be explained by (21). And (21) may be a key to help us realize the action of dielectric loading on the resonance performance of an FSS

## 6. CONCLUSION

Dielectric is one of the most important factors to determine the frequency behavior of FSS. This study showed that for an FSS structure in a given dielectric loading form, there is a transmission upper limit for each plane-wave incidence. It was observed that it is impossible to obtain a higher transmission than the upper limit by designing the array and element of FSS. The transmission upper limit for single-layer FSS with an infinitely thin array is present as (21). This transmission upper limit was found to be independent of the solution technique, which was proved by both theoretical analysis and experiments.

The transmission upper limit presented in this paper describes the possible degree of the effect of dielectrics on the frequency response of FSS. The expression of this upper limit is much simple and easy to compute, which makes it possible to make a rapid evaluation of different dielectric loading plans in the design of FSS. This result might also be helpful for realizing the mechanism of loss and reflection in FSS structure.

## ACKNOWLEDGMENT

The authors would like to thank the National Natural Science Foundation of China, Grant No. 90305026.

## REFERENCES

1. Vardaxoglou, J. C., *Frequency Selective Surfaces Analysis and Design*, Chaps. 1 & 2, John Wiley & Sons, Inc., New York, 1997.
2. Munk, B. A., *Frequency Selective Surfaces Theory and Design*, 1–25, 109–112, John Wiley & Sons, New York, Inc., 2000.
3. Topsakal, E. and J. L. Volakis, “On the properties of materials for designing filters at optical frequencies,” *IEEE Antennas and Propagation Society International Symposium*, Vol. 4, 635–638, Jun. 22–27, 2003.

4. Chandran, S. and J. C. Vardaxoglou, "Performance of two single-layer frequency-selective surfaces as spatial filters," *Microwave and Optical Technology Lett.*, Vol. 6, 339–342, 1993.
5. Lee, D., S. Chakravarty, and R. Mittra, "Design of dual band radomes for high off-normal incidence using frequency selective surfaces embedded in dielectric media," *Electronics Lett.*, Vol. 36, 1551–1552, Aug. 2000.
6. Wahid, M. and S. B. Momis, "Band pass radomes for reduced RCS," *IEE Colloquium on Antenna Radar Cross Section*, 4/1–4/9, May 1991.
7. Mittra, R., C. H. Chan, and T. Cwik, "Techniques for analyzing frequency selective surfaces — A review," *Proceedings of the IEEE*, Vol. 76, No. 12, 1593–1615, Dec. 1988.
8. Luebbers, R. and B. A. Munk, "Some effects of dielectric loading on periodic slot arrays," *IEEE Transactions on Antennas and Propagation*, Vol. 26, 536–542, Jul. 1978.
9. Munk, B. A. and R. D. Fulton, "Transmission through a bi-planar slot array sandwiched between three dielectric layers," Tech. Rept. 3622-7, Electro Science Lab., Dept. of Electric Eng., Ohio State Univ., Columbus, Feb. 1976.
10. Callaghan, P., E. A. Parker, and R. J. Langley, "Influence of supporting dielectric layers on the transmission properties of frequency selective surfaces," *IEE Proceedings on Microwaves, Antennas and Propagation*, Vol. 5, 448–454, Oct. 1991.
11. Wu, T. K., *Frequency Selective Surface and Grid Array*, 7–9, John Wiley & Sons, Inc., New York, 1995.
12. Kontogeorgos, A. A., D. P. Korfiatis, and K. A. Th. Thoma, and J. C. Vardaxoglou, "Plasma generation in silicon-based inductive grid arrays," *Optics and Lasers in Engineering*, Vol. 47, 1195–1198, Nov. 2009.
13. Doumanis, E. T., J. C. Vardaxoglou, D. P. Korfiatis, and K. A. Th. Thoma, "Integrated Schottky-contact in 2-layer inductive grid array," *The Second European Conference on Antennas and Propagation*, 1–6, Nov. 2007.
14. Bossard, J. A., X. T. Liang, L. Li, S. Yun, D. H. Werner, et al., "Tunable frequency selective surfaces and negative-zero-positive index metamaterials based on liquid crystals," *IEEE Transactions on Antennas and Propagation*, Vol. 56, 1308–1320, May 2008.
15. Bossard, J. A., S. Yun, Y. Tang, J. A. Smith, D. H. Werner, et al., "Multiband all-dielectric frequency selective surface filters for the mid-infrared," *Proceeding of the 2007 IEEE Antennas and*

- Propagation International Symposium*, 3416–3419, Jun. 2007.
16. Coves, A., B. Gimeno, J. Gil, M. V. Andrés, A. A. San Blas, et al., “Full-wave analysis of dielectric frequency-selective surfaces using a vectorial modal method,” *IEEE Transactions on Antennas and Propagation*, Vol. 52, 2091–2098, Aug. 2004.
  17. Kristensson, G., A. Akerberg, and S. Poulsen, “Scattering from a frequency selective surface supported by a Bianisotropic substrate,” *Progress In Electromagnetics Research*, Vol. 35, 83–114, 2002.
  18. Zhang, J. C., Y. Z. Yin, and R. P. Yi, “Resonant characteristics of frequency selective surfaces on ferrite substrates,” *Progress In Electromagnetics Research*, Vol. 95, 355–364, 2009.
  19. Yang, L. and S. Xu, “Investigation into effects of dielectric loss on frequency selective characteristics of dielectric periodic structures,” *IEE Pro.-Microw. Antenna Propag.*, Vol. 148, Oct. 2001.
  20. Bossard, J. A., D. H. Werner, T. S. Mayer, J. A. Smith, Y. U. Tang, et al., “The design and fabrication of planar multiband metallodielectric frequency selective surfaces for infrared applications,” *IEEE Transactions on Antennas and Propagation*, Vol. 54, 1265–1276, Apr. 2006.
  21. Zareian-Jahromi, E. and M. Shahabadi, “Investigation of the effect of conductor loss and mismatch on the tunneling through frequency selective surfaces,” *International Conference on Microwave and Millimeter Wave Technology*, Vol. 2, 535–538, Apr. 2008.
  22. Barlevy, A. S. and S. Y. Rahmat, “Analysis of arbitrary frequency selective surfaces: Analytic constraints,” *Antennas and Propagation Society International Symposium*, Vol. 2, 1440–1443, Jul. 1996.
  23. Chen, C. C., “Scattering by a two-dimensional periodic array of conducting plates,” *IEEE Transactions on Antennas and Propagation*, Vol. 5, 660–665, Jul. 1970.
  24. Wu, Z. B., “Research on essential problems of electrical performance analysis for FSS stealth radome,” Ph. D. dissertation, School of Aeronautic Science and Technology, Beijing University of Aeronautics and Astronautics, Beijing, China, 2004.
  25. Lomakin, V. and E. Michielssen, “Transmission of transient plane waves through perfect electrically conducting plates perforated by periodic arrays of subwavelength holes,” *IEEE Transactions on Antennas and Propagation*, Vol. 54, 970–984, Mar. 2006.

26. Kirilenko, A. A. and A. O. Perov, “On the common nature of the enhanced and resonance transmission through the periodical set of holes,” *IEEE Transactions on Antennas and Propagation*, Vol. 56, 3210–3216, Oct. 2008.